scientific reports

OPEN

Electron temperature and density measurement by Thomson scattering with a high repetition rate laser of 20 kHz on LHD

H. Funaba[1✉], R. Yasuhara[1✉], H. Uehara[1], I. Yamada[1], R. Sakamoto[1], M. Osakabe[1] & D. J. Den Hartog[2]

Thomson scattering measurements with a high-repetition-rate laser have commenced in the Large Helical Device. As an example of the fast phenomena captured by this diagnostic system, measurements at a 20 kHz repetition-rate in hydrogen pellet-injected plasmas are presented. Signal processing methods for this measurement have been developed and electron temperature profiles with almost 70 spatial points were evaluated at time intervals of 50 µs. After Raman scattering calibration, electron density profiles were derived. Fast changes in the electron temperature and density profiles within 1 ms were observed.

For magnetically confined fusion devices, electron temperature (T_e) and electron density (n_e) are fundamental parameters of plasmas. Thomson scattering diagnostics is a widely adopted measurement method of T_e and n_e in fusion plasma devices[1–17] because of the reliability of the results and no perturbation for the plasma. Since the cross-section of Thomson scattering, σ_T, is almost 6.65×10^{-29} m^2, pulsed lasers with an energy of a few joules are usually used for this measurement. The Salpeter parameter, α, determines whether the scattering is non-collective or collective. α is defined by $\alpha \equiv 1/(|\boldsymbol{k}|\lambda_D)$, where $\boldsymbol{k}$ and λ_D are the scattering wavenumber and Debye length, respectively. When $\alpha \ll 1$, the scattering is non-collective. In this case, the spectrum of the scattered light reflects T_e and the intensity is related with n_e. It is possible to obtain a spatial profile of T_e and n_e by applying the suitable geometry of laser injection and light collection optics.

In plasmas fast phenomena are frequently observed, such as magnetohydrodynamic (MHD) instabilities, solid pellet injection and so on. It is required to measure the fast change of plasma parameters for understanding of these phenomena. In order to measure the temporal development of T_e and n_e during fast phenomena, a laser operation with short time intervals between pulses is used for Thomson scattering measurements. One way to realize such short intervals is to use several lasers. Three Nd:YAG (neodymium-doped yttrium aluminum garnet) lasers are used in the Thomson scattering system[1,2] in the Large Helical Device (LHD)[18,19]. For a pellet-injected plasma, two of them were pulsed with a short interval of 200 µs[20]. For the same purpose, Thomson scattering diagnostic systems with high-repetition-rate lasers have been developed in W7-X with 12 burst pulses on a 5 Hz basis[21]. Profiles of T_e and n_e were obtained with a time interval of 100 µs during the injection process of a cryogenic H$_2$ pellet. Multi-pass Thomson scattering (MPTS) is one of the methods to increase an effective signal intensity of the scattered light. At the same time, with this method it is also considered that a quite fast time resolution is achieved, since the interval of multi-pass signals is shorter than 100 ns in the case of the Thomson scattering system in GAMMA10/PDX[22,23]. The double-pass intracavity ruby laser system was developed in TEXTOR and a train of 20 laser pulses with 10 kHz were produced[24]. A laser which has a repetition-rate of the order of 1 kHz is suitable for the measurement in magnetically confined plasma devices which have a duration of a few tens of milliseconds. In the Thomson scattering system in VEST, T_e and n_e at ten time points are measured during a typical plasma duration of about 20 ms, using a laser with a repetition-rate of 1 kHz[17]. Recently, Thomson scattering measurements with a high-repetition-rate Nd:YAG laser started in LHD. This laser was newly developed by a collaboration of National Institute for Fusion Science (NIFS) and the University of Wisconsin-Madison, based on a "pulse-burst" laser system[25–27] and can be operated with a repetition frequency up to 20 kHz. Temporal development of the spatial profiles of T_e were derived and n_e profiles were also evaluated after the

[1]National Institute for Fusion Science, National Institutes of Natural Sciences, Toki, Gifu 509-5292, Japan. [2]Department of Physics, University of Wisconsin-Madison, Madison, WI 53706-1390, USA. ✉email: funaba.hisamichi@nifs.ac.jp; yasuhara.ryo@nifs.ac.jp

density calibration by Raman scattering. A pulse-burst laser system for Thomson scattering measurement was also developed in the University of Tennessee[28].

In this study, signal processing from the data acquisition to the evaluation of T_e and n_e with a high-repetition-rate laser is established. This diagnostic is applied for a plasma with solid hydrogen pellet injection as one of the fast transient phenomena in plasmas. Then it is intended to observe fast changes in the T_e and n_e profiles with a temporal resolution of 50 μs.

This paper consists of three major sections: Introduction, Results, and Summary before the Methods section. The Results section is divided into four sub-sections as follows: (1) "Experimental setup", (2) "Electron temperature profiles in a pellet-injected plasma", (3) "Raman scattering calibration", and (4) "Electron density profiles".

(1) The "Experimental setup" consists of three parts of the "Thomson scattering diagnostic system in LHD", "The new high-repetition-rate Nd:YAG laser", and "Switched-capacitor-type fast digitizers" which describe the LHD Thomson scattering system, a high-repetition-rate Nd:YAG laser and the fast digitizers for it , respectively. In sub-section (2) "Electron temperature profiles in a pellet-injected plasma", abrupt changes in a plasma are described in the sub-subsection "Plasma parameters of a pellet-injected plasma". Signals of the Thomson scattering diagnostics and their time-integration are shown in "Signal processing for fast digitizers". T_e profiles in the pellet-injected plasma are presented in "Electron temperature profiles" as an example of the fast change of T_e. (3) The "Raman scattering calibration" sub-section describes the electron density calibration process and the results of the calibration. In (4) "Electron density profiles", the fast change of n_e profiles in the pellet-injected plasma is shown and the validity of the measured n_e is discussed. The Summary section is a brief synopsis of this work. The Methods section contains a description of LHD.

Results

In this section, at first the experimental setup is described. The new laser and fast digitizer boards are explained in brief. Then the data processing methods and an example of fast temporal development of T_e are shown. In order to derive n_e, the results of Raman scattering calibration are described. Lastly, the results of n_e profiles by the new laser are shown for the first time.

Experimental setup. *Thomson scattering diagnostic system in LHD.* The Thomson scattering diagnostics system in LHD consists of the following components: lasers and the laser transfer and injection optics into the plasma, the collection and transfer optics of scattered light, the detection system of the spectrum by polychromators, the analog-to-digital conversion (ADC) of the signals, and the analysis system of T_e and n_e. Nd:YAG lasers are used and the laser light is transferred by mirrors to LHD for almost 40 m. The laser pulses are injected horizontally into the equatorial plane of LHD and backscattering light is observed. The scattering angle is almost 167° at the center of the plasma. The Salpeter parameter α is $\alpha \ll 1$ even in low T_e and high n_e conditions, for example, $\alpha \simeq 1.1 \times 10^{-2}$ for $T_e = 100$ eV and $n_e = 10^{20}$ m^{-3}. Therefore, a non-collective scattering condition is applied. The scattered light is collected and focused on the ends of optical fibers by a large concave mirror coated in gold. Then the light is transferred by the optical fibers to the inlets of the polychromators.

The main Thomson scattering system in LHD has three Nd:YAG lasers, one of which is operated at 30 Hz and the other two at 10 Hz. The laser pulses can be injected into the plasma simultaneously or separately. The number of spatial positions is 144 for the main system. A polychromator consists of five or six filter channels for spectroscopic measurement of the scattered light. In the main system, charge integration type ADCs, FASTBUS, are used.

In addition to the main system, a new Nd:YAG laser with a high-repetition-rate and fast digitizers of the switched-capacitor-type are newly installed. An output signal of one polychromator channel is amplified and separated in two. One of them is detected by the FASTBUS system, and the other output is used for checking of the signals by oscilloscopes or connected to the newly installed digitizers.

The new high-repetition-rate Nd:YAG laser. The new high-repetition-frequency Nd:YAG laser in LHD was developed under the collaboration of NIFS and the University of Wisconsin-Madison, based on a "pulse-burst" laser system. This laser can be operated with two kinds of repetition frequencies, one of which is 1 kHz with 30 laser pulses and the other is 20 kHz with 100 laser pulses. Therefore, the time range of the measurement is 30 ms and 5 ms for the 1 kHz and 20 kHz cases, respectively. The typical energy of the laser pulse is 1.6 J for the 1 kHz operation and almost $1 \sim 1.2$ J for the 20 kHz operation. The signals of the laser pulses during the operation are monitored in the 1 kHz case, while they are not obtained yet in the 20 kHz case.

Switched-capacitor-type fast digitizers. The scattered light from the plasmas is detected by polychromators and the AC component of the signal is amplified. Then the signals are acquired by the ADC. Since the frequency of the high-repetition-rate laser is up to 20 kHz, it is necessary to acquire the data with an interval of 50 μs. The charge-integration type detector is not suitable for the measurement with such a short interval, because several time gates for the signal frame and some background frames are needed. Therefore, new multi-channel fast digitizer boards of a switched-capacitor-type, TechnoAP APV85G32L, were installed. One board of this digitizer has 32 channels of inputs and acquires data with a sampling frequency of 1 GS/s. The minimum read-out time which is needed to convert analog to digital in these switched-capacitor-type digitizers, is shorter than 50 μs. The number of spatial positions measured by this new digitizer system is almost 70 with the 12 boards.

This fast digitizer includes 4 DRS4 (Domino Ring Sampler)[29] chips which are switched-capacitor arrays. Each channel has 1024 storage cells. In the 1 kHz operation of the laser, the length of the data is 1024 points, while it becomes 256 points in the 20 kHz operation. The data which are acquired by the DRS4 need some corrections, such as the cell amplitude calibration which corrects the difference of the amplitude of the capacitors, the peak
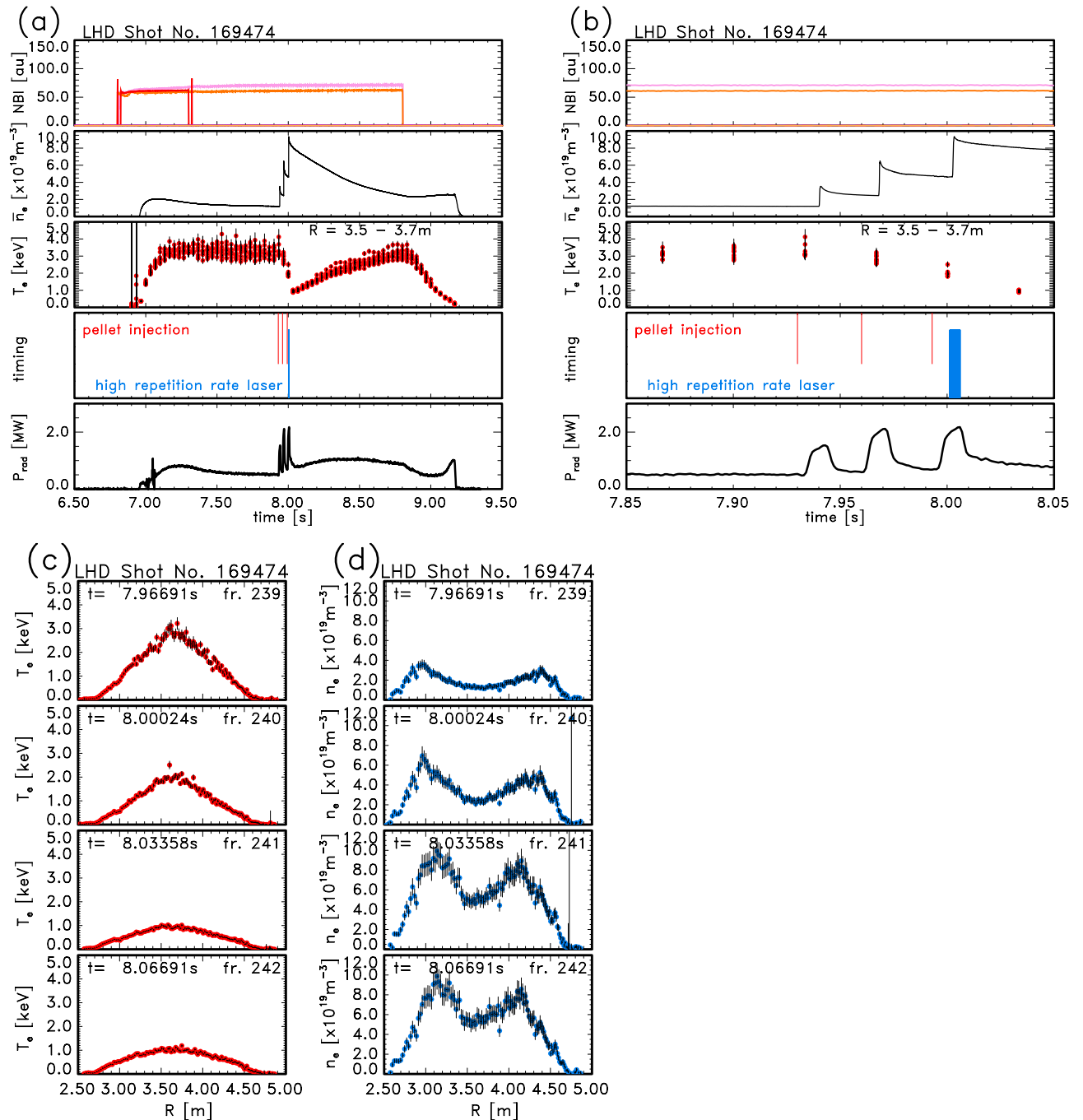
Figure 1. Some plasma parameters in a solid pellet-injected plasma. The temporal development of NBI heating pulses, line-averaged electron density ($\bar{n}_e$), T_e, timings of pellets (red) and laser pulses of the high-repetition-rate laser (blue), and radiation power (P_{rad}) and the T_e and n_e profiles in a pellet-injected plasma in LHD. These T_e and n_e profiles are measured by a laser with a repetition frequency of 30 Hz. (**a**) the whole time of the plasma, (**b**) the expanded time around the pellet injection, (**c**) T_e profiles, and (**d**) n_e profiles.

correction of which removes a few spikes with one or two points appearing at the same timing among the DRS4 channels, and so on. The peak correction can be made by interpolation.

Electron temperature profiles in a pellet-injected plasma. *Plasma parameters of a pellet-injected plasma.* In this subsection, methods of the signal processing for the switched-capacitor-type digitizers and the evaluation of T_e are described. As an example of fast changes of plasma parameters, a hydrogen pellet-injected plasma is shown. Figure 1a shows the temporal development of some plasma parameters such as neutral beam injection (NBI) heating pulses, line-averaged electron density ($\bar{n}_e$) which was measured by a far infrared (FIR) interferometer, T_e around the plasma center by Thomson scattering with a 30 Hz laser, timings of pellets and the new laser, and radiation power (P_{rad}) in an LHD plasma where three solid hydrogen pellets were injected by the
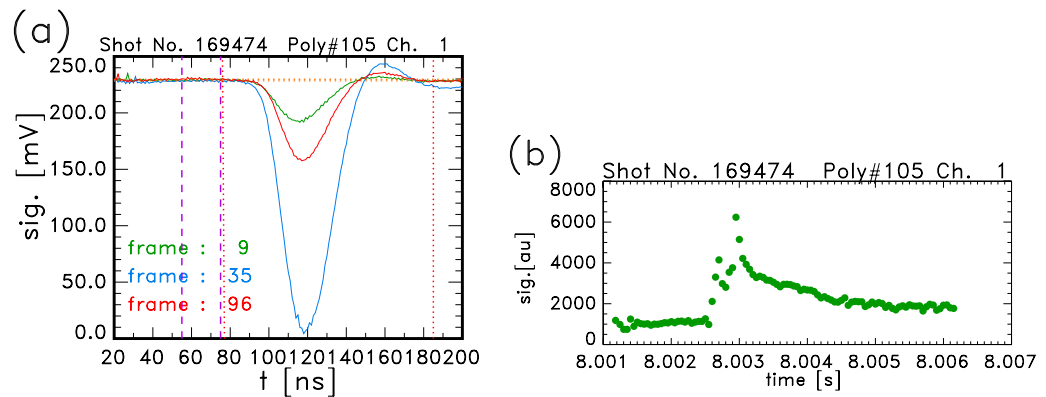
Figure 2. Signals of Thomson scattering measurement. (**a**) Examples of the signals of Thomson scattering in a pellet-injected plasma. Frames Nos. 9, 35 and 96 correspond to $t = 8.00165, 8.00295$ and 8.00600 s, respectively. (**b**) Temporal development of an integrated signal. The abscissa represents the same time as in Fig. 1.

LHD pellet injector[30]. The abscissa of Fig. 1b is an expansion of Fig. 1a around the pellet injection timings. Since the timing lines of the pellets (red) are based on signals from the pellet injection system, they are almost 10 ms earlier than the actual injection timings. The laser timings of the high-repetition-rate laser are also shown in Fig. 1a, b. 100 laser pulses were injected within 5 ms around $t = 8.0$ s ($t = 8.00120 \sim 8.00615$ s). The timing of the first laser pulse is just before the actual injection of the third pellet. The temporal development of the spatial profile of T_e is shown in Fig. 1c and that of n_e profiles is shown in Fig. 1d. The abscissa, R, is the major radius of the torus plasma. These T_e and n_e profiles are measured by the Thomson scattering with a laser of a repetition frequency of 30 Hz. The n_e profile at $t = 7.96691$ s has already become hollow due to the first pellet.

In Fig. 1c, $T_e \simeq 3$ keV in the center region at $t = 7.96691$ s is the timing before the second pellet reached the plasma. The timing of 8.00024 s is just before the actual injection of the third pellet. Although the T_e and n_e significantly changed between $t = 8.00024$ and 8.03358 s, detailed change cannot be known from this laser frequency. It is considered that the profiles mainly changed within 1 ms from the previous results. After the pellet injection, a plasmoid component is formed[31,32] in the background plasma. The pellets are injected into a horizontally elongated cross-section of the plasma. Since the difference of the toroidal angle between the pellet injection and the Thomson scattering diagnostics is $\frac{1}{5}\pi$, there may be a possibility that the plasmoid component can be measured by the Thomson scattering system. The timings when such a plasmoid may exist were not included in Fig. 1d.

Signal processing for fast digitizers. Figure 2a shows some signals of Thomson scattering measurement which were acquired by the new switched-capacitor-type digitizers, APV85G32L, in the same pellet-injected plasma of Fig. 1. Cell amplitude calibration and a peak correction were made. These signals were detected from polychromator No. 105 (Poly#105), which observes at the major radius position of $R = 4.376$ m. This position is located almost in the middle of the outside of the magnetic axis. The usual polychromator has five spectral channels for the Thomson scattering measurement. The data of channel 1, which is the closest channel to the laser wavelength, are shown here. The frame number i corresponds to the signal by the $(i + 1)$th laser pulse. The frames Nos. 9, 35 and 96 correspond to $t = 8.00165, 8.00295$ and 8.00600 s, respectively.

In order to derive T_e and n_e, precise evaluation is needed in the following processes. These are the evaluation of the background level, the determination of the signal gate timing, the time-integration of the signals, and the subtraction of stray light. The background level is derived by averaging the data just before the signal, which is indicated by the region between the purple broken lines in Fig. 2a. The gate timing where the time integration is made is shown between the red dotted lines. The width of this gate is 110 ns and the timing is adjusted for each polychromator. The time-integration is made by a simple summation of the data in this gate timing, as the first step of the analysis. The stray light component is estimated from the signal, which is acquired without the plasma, and it is subtracted after the integration. In the case of Fig. 2a, the stray light component is quite small. Figure 2b shows the temporal development of the signal intensity of channel No. 1 of Poly#105. The value of the signal is obtained from the product of the voltage and time in the units of [mV] and [ns], respectively. On the other hand, it is found that the estimated number of detected photons in one channel of the polychromator may be in a similar order of the value of the integrated signal. Then this value is considered to be related with the number of photons and the unit here is expressed by [au]. The abscissa represents the same time in Fig. 1. The relative energy of each laser pulse is estimated from the signal of the laser pulse for the 1 kHz operation. However, since it is not yet observed in the 20 kHz operation because of the short time range of 255 ns, constant energy is assumed for the 20 kHz case. The intensity increased after frame No. 28, which corresponds to $t = 8.00260$ s, and it became quite large at frame No. 35 ($t = 8.00295$ s), but saturation of the signal was not found.

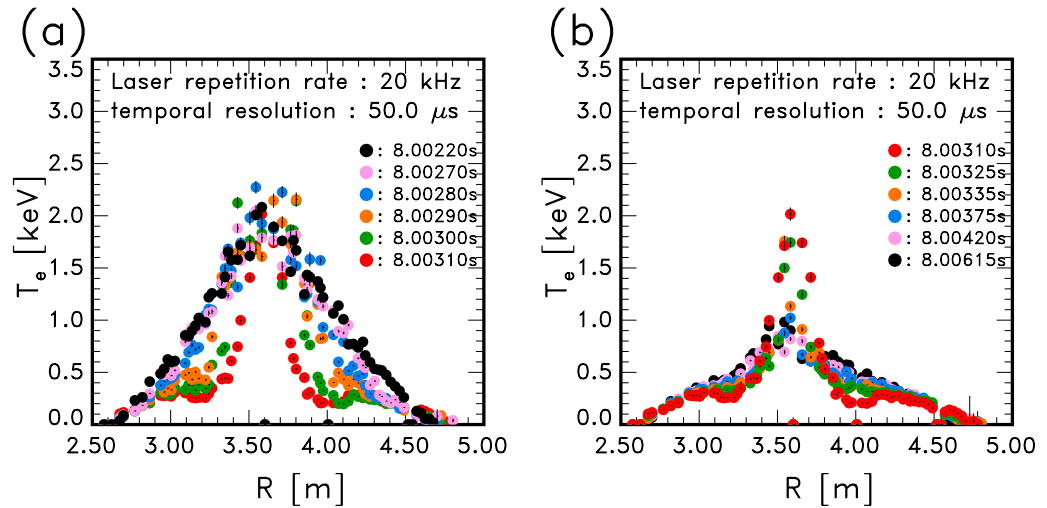*Electron temperature profiles.* The electron temperature is evaluated by the χ^2-method which minimize the following χ^2,

Figure 3. Temporal development of T_e profiles in a pellet-injected plasma. (**a**) $t = 8.00220 \sim 8.00310$ s, (**b**) $t = 8.00310 \sim 8.00615$ s.

$$\chi^2 = \sum_i w_i (x_i - \lambda_c s_i)^2, \tag{1}$$

where i represents i-th channel of a polychromator and x_i, s_i, w_i, λ_c are the signal intensity, the expected intensity for the specific T_e, the weight and a constant coefficient, respectively. The error of T_e is evaluated from the T_e region which provides χ^2 under $\chi^2_{min} + \Delta\chi^2$, where χ^2_{min} denotes the minimum χ^2. When the shot noise is considered to be a main cause of the error, $\Delta\chi^2 = 1$ can be used with w_i, which corresponds to the inverse of the magnitude of the signals. For the first analysis, constant $w_i = 0.001$ is assumed for all channels in order to avoid that the magnitude of weight becomes unstable when the signal is small. This weight is chosen because the value of the integrated signal is usually in the range of 100 $\sim$ 3000. The results of T_e are similar to those from the 30 Hz laser which are evaluated with w_i, considering the shot noise and fluctuation of the background light. The time-integrated signals are used as x_i. In order to confirm the validity of T_e profiles, the signals and temporal evolution of T_e in almost constant T_e plasmas were checked.

Figure 3 shows the temporal development of the T_e profiles which were obtained in the same plasma as in Fig. 1. The position of the magnetic axis in a vacuum was $R = 3.60$ m. The number of spatial positions was almost 70 in these profiles. Some selected timings when the T_e profiles were clearly distinguishable are shown here, although the actual time resolution was 50 μs. The T_e profile at the first timing $t = 8.00220$ s (*black circles*) was almost the same as that at $t = 8.00024$ s in Fig. 1c. The pellet was injected from outside of the torus. T_e decreased from the outside of the plasma, while T_e at the center region still remained high until $t = 8.00310$ s. Thus, the T_e profile changed within 1 ms. It was found that the time interval of 50 μs had enough temporal resolution. From the results of T_e profiles between $t = 8.00310$ and 8.00615 s in Fig. 3b, T_e at the center decreased and T_e around $R \simeq 3.2$ and 4.0 m gradually recovered.

Raman scattering calibration. The results of the electron density calibration by Raman scattering for the Thomson scattering diagnostics with the high-repetition-rate Nd:YAG laser are shown in this subsection. Figure 4 shows the data of the Raman scattering calibration, which was made by filling the vacuum vessel with dry air. The data were obtained in the same channel of Fig. 2 and the laser was in the 1 kHz operation. The *green data* are the temporal development of the integrated signal of Raman scattering and the *yellow data* are those of the laser signals, which correspond to the energy of the laser pulses. The red line indicates the average of these data. The number of laser pulses used in the averaging is 30 in the 1 kHz case and 100 in the 20 kHz case, which are the numbers in one series of laser operation. The *magenta data* are the Raman data which are normalized by the laser power. The fluctuation of the laser power is not large except for the first pulse. A few data just after the start of the laser become small, although the laser power is not small. The reason for this is not clear at present. The scattering of these data may be larger than the actual Raman data, since the noise components which were caused by the digitizers remained, although corrections were made. However, it is considered that the effects of such noises may be small in high densty cases like pellet injection experiments. In this paper, the temporal integration of signals is made simply by a summation as the first step of the analysis. However, it is considered that the effects of such noise components can be removed by signal processing. For the 20 kHz operation, the laser power is not obtained and it is assumed to be constant in the analysis.

Figure 5 shows the dependence of the averaged Raman signal intensity, which is shown by the red line in Fig. 4, on the pressure, P. The Raman data were obtained under $P \simeq 3 \times 10^4$ Pa. As the value of y-intercept of the linear approximation, b, is small enough, the gradient of this relation, a, is used for the density calibration. The intensity of Raman scattered light in the spectral channel No. 1, S_1^R, is expressed by
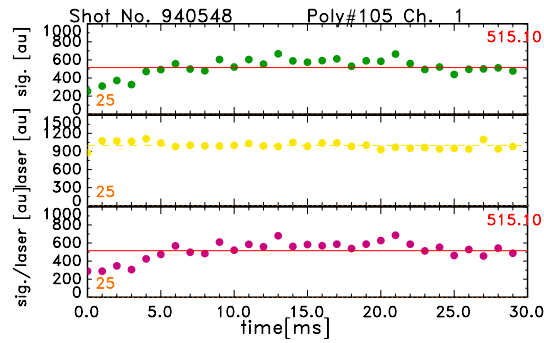
5

Figure 4. Data of Raman scattering. The *green data* are the temporal development of the integrated signal of Raman scattering in the 1 kHz operation of the laser. The *yellow data* are those of the laser signal. The red line indicates the average of these data. The *magenta data* are the Raman data which are normalized by the laser power.
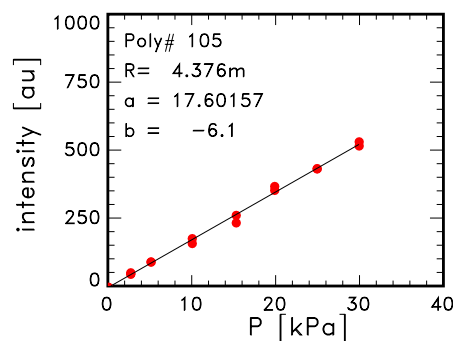

Figure 5. Results of Raman scattering calibration. Relation of the averaged Raman signal intensity and pressure. *a* and *b* are the gradient and y-intercept of the linear approximation.

$$S_1^R = aP + b \simeq aP = an_0kT_0, \tag{2}$$

where n_0, k, and T_0 are the neutral density of the air, the Boltzmann constant and the room temperature, respectively.

The signal intensity of Thomson scattering for the spectral channel No. i, S_i^T, and that of Raman scattering for the spectral channel No.1 , S_1^R, are expressed as follows[33].

$$S_i^T = AP_L n_e \int \sigma^T(T_e, \lambda) f_i(\lambda) d\lambda \frac{dI^T}{d\Omega} \tag{3}$$

$$S_1^R = AP_L \left[n^N \sum_J w_J^N \sigma_J^N(\lambda_J^N) f_1(\lambda_J^N) + n^O \sum_J w_J^O \sigma_J^O(\lambda_J^O) f_1(\lambda_J^O) \right] \frac{dI^R}{d\Omega}, \tag{4}$$

Here A is a common coefficient in Thomson and Raman scattering, P_L is the energy of the laser pulse, and λ is the wavelength. In Eq. (3), σ^T is the cross-section of Thomson scattering, f_i is the spectral responsibility of channel No.i, and $\frac{dI^T}{d\Omega}$ is the angular distribution of Thomson light. In Eq. (4), J is the initial rotational-angular-momentum quantum number, $w_J^{N,O}$ is the population of the initial rotational state, and $\sigma_J^{N,O}$ is the cross-section of the anti-Stokes rotational $J' = J - 2$ Raman transition. 'N' and 'O' represent nitrogen and oxygen, respectively. $\frac{dI^R}{d\Omega}$ is the angular dependence of the differential cross-section of the quadrupole Raman transition.

Figure 6 shows the wavelength dependence of the transparency of the filters in Poly#105 and the cross-sections of the Raman scattering for molecular nitrogen (green circle) and oxygen (red circle). The Raman signal is mainly detected by channel No. 1 (cyan curve). By using the ratio of nitrogen and oxygen, $r^N = n^N/n_0$ and $r^O = n^O/n_0$, respectively, the effective Raman cross-section, σ_{eff}^R is defined as

$$\sigma_{eff}^R = r^N \sum_J w_J^N \sigma_J^N(\lambda_J^N) f_1(\lambda_J^N) + r^O \sum_J w_J^O \sigma_J^O(\lambda_J^O) f_1(\lambda_J^O), \tag{5}$$
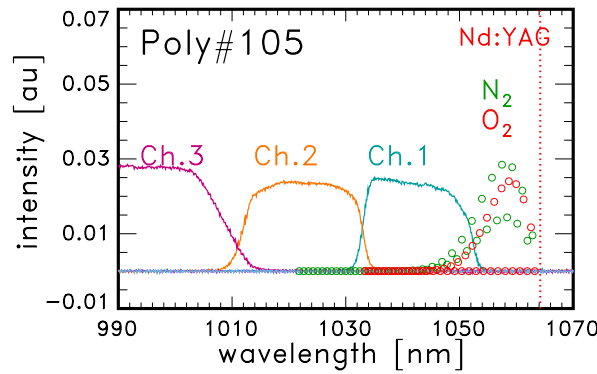
and Eq. (4) is written as

Figure 6. Raman coefficients and the polychromator channels. Wavelength dependence of the transparency of the filters in polychromator No. 105 and cross-sections of the Raman scattering for molecular nitrogen (*green circles*) and oxygen (*red circles*). The red dotted line at 1064 nm shows the wavelength of the Nd:YAG laser.
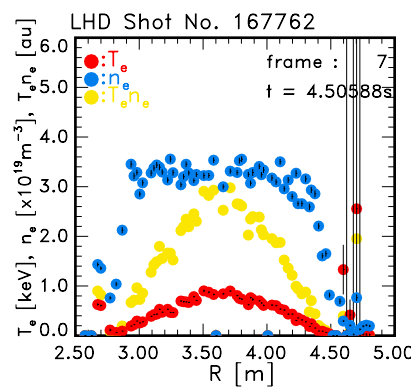

Figure 7. Confirmation of the validity of the electron density measurement. An example of n_e profiles in a plasma with a relatively flat shape. The data were acquired in the 1 kHz opertion. n_e (*blue circles*), T_e (*red circles*), and the product of $n_e T_e$ (*yellow circles*) are shown.

$$S_1^R = AP_L n_0 \sigma_{\text{eff}}^R \frac{dI^R}{d\Omega} = an_0 kT_0. \tag{6}$$

Here the relation of Eq. (2) is used. The total intensity of Thomson scattering signals in a polychromator is expressed by

$$\sum_i S_i^T = AP_L n_e \sum_i \int \sigma^T(T_e, \lambda) f_i(\lambda) d\lambda \frac{dI^T}{d\Omega}. \tag{7}$$

Then n_e is evaluated by Eq. (7) where A is derived from Eq. (6). The difference of laser power between the 1 kHz and 20 kHz operations is included in the Raman coefficients for the electron density calibration.

Electron density profiles. In this subsection the n_e profiles, which are calculated with the Raman calibration data, are shown. In order to confirm the validity of the calibration, the n_e profile of a plasma with $n_e \simeq 3 \times 10^{19}$ m^{-3} is shown in Fig. 7 as *blue closed circles*. The T_e profile (*red circles*) and the product of $n_e T_e$ (*yellow circles*) are also shown in the same figure. The data were acquired in the 1 kHz operation of the laser. The n_e profile in this plasma was relatively flat and almost the same n_e value and profile was also observed by the Thomson scattering measurement with the 30 Hz laser, where the n_e calibration was made independently. The line-averaged electron density by the FIR interferometer was almost 2.6×10^{19} m^{-3}, while the averaged value of n_e in Fig. 7 along the laser line was almost 2.8×10^{19} m^{-3}. Here only the effect of the shot noise is considered as an error of n_e, since the estimation of the scattering of the Raman data may be too large, because of the noises from the digitizers.

Temporal development of the n_e profile of the pellet-injected plasma is shown in Fig. 8a–g. The marks are the same as in Fig. 7, that is, n_e, T_e and $T_e n_e$ are indicated by *blue*, *red* and *yellow closed circles*, respectively. n_e started to increase at $t = 8.00275$ s (Fig. 8b) from the outside of the torus. Since the velocity of the pellet was almost 1 km/s, it is considered that it progressed about 1 m in 1 ms. The low T_e region where $T_e \leq 0.3$ keV seemed to penetrate into the center region of the plasma. In Fig. 8c, quite high n_e was observed in the torus outer region.
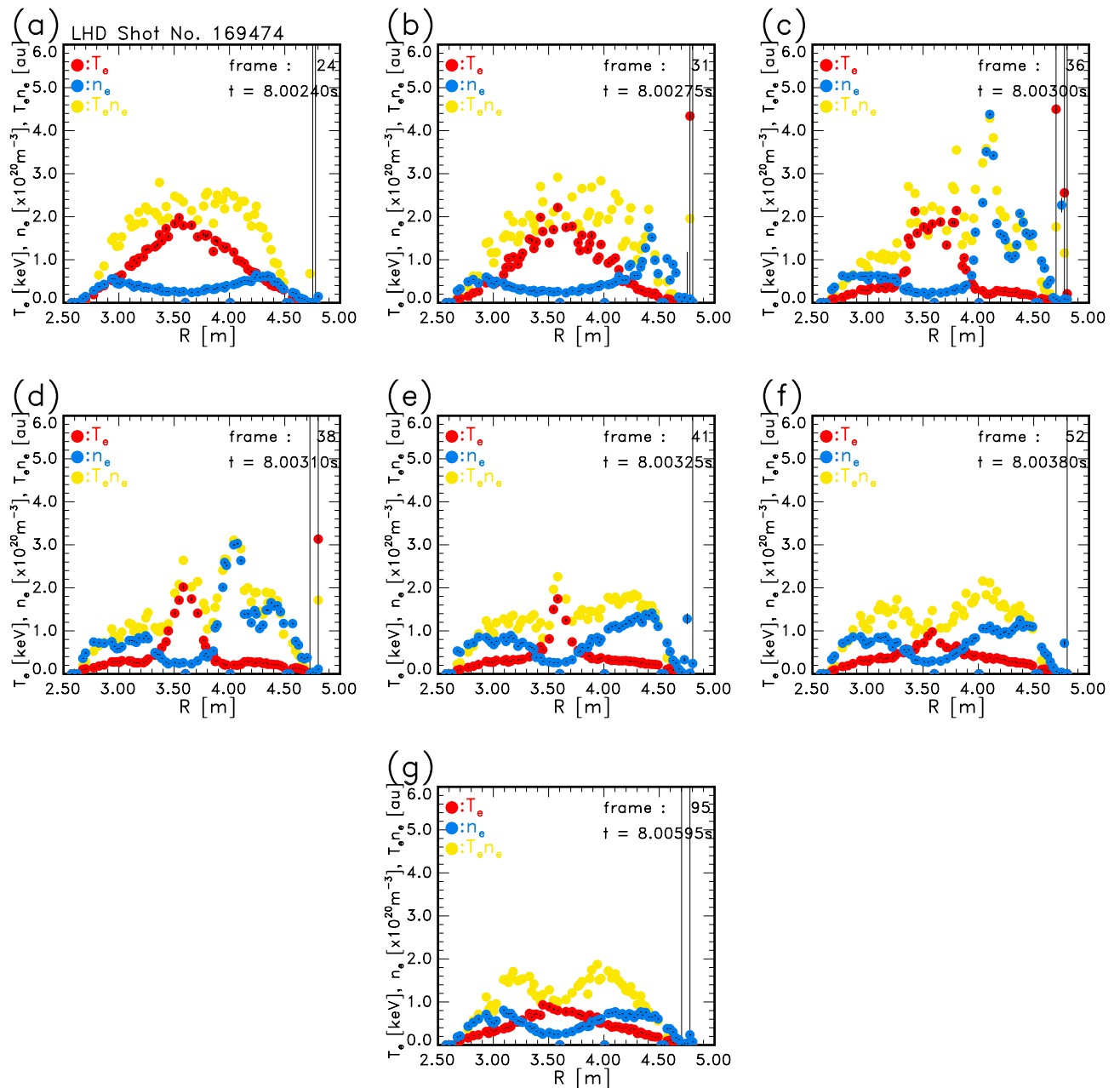
Figure 8. Temporal development of the n_e profile of the pellet-injected plasma which was measured by the 20 kHz operation of the laser. n_e (*blue circles*), T_e (*red circles*) and the product of $n_e T_e$ (*yellow circles*) are shown.

The pellet seemed to vanish by ablation at $t = 8.00310$ s (Fig. 8d) because the low T_e region stopped penetrating. In the spatial profiles of n_e and even in $n_e T_e$, asymmetry between the inner and the outer side of the magnetic axis was found during the pellet ablation time. The reason for this asymmetry is considered because these spatial profiles of n_e also contain the plasmoid component, which is formed by the pellet ablation, in addition to the background electron density. From Fig. 8e–g, the n_e profile seems to show recovery of the symmetry. A similar T_e profile with a steep gradient at the center like Fig. 8d and high n_e in the outer region, like Fig. 8c,d, are already observed[20]. However, the gradual change of the T_e and n_e within 1 ms is observed for the first time in the pellet-injected plasma in LHD.

Summary

Thomson scattering diagnostics with a high-repetition-rate laser, which can be operated up to 20 kHz, have started in LHD. Some processes for analyzing the Thomson scattered signals with the temporal development is established, such as the determination of the background level, the gate timings for the time-integration, the temporal integration method and so on. In this first analysis, the temporal integration was made by simple summation.

n_e calibration by Raman scattering was made. The evaluated n_e profiles show valid results for plasmas with a relatively flat shape. The first results of the temporal evolution of T_e and n_e profiles in a pellet-injected plasma are shown. The penetration of the low T_e region into the center of the plasma and a quite high n_e region, which consists of the plasmoid component and background plasma, is formed outside of the torus. The temporal development of T_e and n_e within 1 ms is observed in detail by these diagnostics.

Methods

The Large Helical Device (LHD).   LHD is a magnetically confined fusion plasma experiment device of a heliotron-type with the poloidal period number $l = 2$ and the toroidal period number $m = 10$. The major radius of the magnetic axis in the vacuum R_{ax} is from 3.5 to 4.1, and the average minor radius, $a \simeq 0.6$ m. LHD consists of many systems, such as superconducting coil systems, power supplies, a helium refrigerator, vacuum pumping systems, plasma heating systems, plasma control systems, plasma diagnostic systems, and so on. The magnetic surfaces for plasma confinement are created by external coils which are made with a superconductor and cooled at liquid helium temperature. Therefore, plasma current is not required for plasma confinement. The plasmas are heated by electron cyclotron resonant heating (ECH), neutral beam injection (NBI), and ion cyclotron resonant heating (ICH). The plasmas are usually started by ECH. Moreover, it is possible to start them up by NBI. As control systems, the divertor system, resonant magnetic perturbation (RMP) field coils, fueling systems, and so on are installed. For fueling, hydrogen, deuterium, helium and other gases are provided by a gas-puff system. Solid cryogenic hydrogen or deuterium are injected into the plasmas by the pellet injector. Various systems for the measurement of the plasma parameters are installed, such as electron temperature and density, ion temperature, radiation power, electric potential, fluctuations, neutron yield, and diagnostics for spectroscopic measurements, impurity injection, high energy ions, measurements for the peripheral plasma, and so on. The typical parameters used in this paper are as follows. The magnetic field strength at the magnetic axis, $B = 2.75$ T, the electron temperature, $T_e = 0.1 \sim$ a few keV, the electron density, $n_e = 0.5 \times 10^{19} \sim$ more than 2×10^{20} m^{-3}.

Data availibility

The data of T_e and n_e profiles in the figures of this paper are available from the LHD experiment data repository at https://www-lhd.nifs.ac.jp/pub/Repository_en.html after reading "Data Rights and Rules" and submitting the "LHD Data Usage and Publication Agreement" form. The other data of this study are available from the corresponding authors upon reasonable request.

References

1. Narihara, K., Yamada, I., Hayashi, H. & Yamauchi, K. Design and performance of the Thomson scattering diagnostic on LHD. *Rev. Sci. Instrum.* **72**, 1122–1125. https://doi.org/10.1063/1.1319368 (2001).
2. Yamada, I. *et al.* Recent progress of the LHD Thomson Scattering System. *Fusion Sci. Tech.* **58**, 345–351. https://doi.org/10.13182/FST10-A10820 (2010).
3. Carlstrom, T. N. *et al.* Design and operation of the multipulse Thomson scattering diagnostic on DIII-D (invited). *Rev. Sci. Instrum.* **63**, 4901–4906. https://doi.org/10.1063/1.1143545 (1992).
4. Barth, C. J., Pijper, F. J., Meiden, H. J. v. d., Herranz, J. & Pastor, I. High-resolution multiposition Thomson scattering for the TJ-II stellarator. *Rev. Sci. Instrum.* **70**, 763–767. https://doi.org/10.1063/1.1149399 (1999).
5. Pasqualotto, R. *et al.* High resolution Thomson scattering for Joint European Torus (JET). *Rev. Sci. Instrum.* **75**, 3891–3893. https://doi.org/10.1063/1.1787922 (2004).
6. Maslov, M., Beurskens, M. N. A., Kempenaars, M. & Flanagen, J. Status of the JET LIDAR Thomson scattering diagnostic. *JINST* **8**, C11009. https://doi.org/10.1088/1748-0221/8/11/C11009 (2013).
7. Scannell, R. *et al.* A 130 point Nd:YAG Thomson scattering diagnostic on MAST. *Rev. Sci. Instrum.* **81**, 10D520. https://doi.org/10.1063/1.3460628 (2010).
8. Zang, Q. *et al.* Development of a Thomson scattering diagnostic system on EAST. *Plasma Sci. Technol.* **12**, 144–148. https://doi.org/10.1088/1009-0630/12/2/04 (2010).
9. Lee, J. H., Oh, S. T. & Wi, H. M. Development of KSTAR Thomson scattering system. *Rev. Sci. Instrum.* **81**, 10D528. https://doi.org/10.1063/1.3494275 (2010).
10. Yamaguchi, T. *et al.* Development of a Thomson scattering system in the TST-2 spherical tokamak. *Plasma Fusion Res.* **5**, S2092. https://doi.org/10.1585/pfr.5.S2092 (2010).
11. Minami, T. *et al.* Design of a new high repetition rate Nd:YAG Thomson scattering system for Heliotron J. *Rev. Sci. Instrum.* **81**, 10D532. https://doi.org/10.1063/1.3496977 (2010).
12. Aftanas, M. *et al.* High-resolution Thomson scattering system on the COMPASS tokamak: evaluation of plasma parameters and error analysis. *Rev. Sci. Instrum.* **83**, 10E350. https://doi.org/10.1063/1.4743956 (2012).
13. Kurzan, B. & Murmann, H. D. Edge and core Thomson scattering systems and their calibration on the ASDEX Upgrade tokamak. *Rev. Sci. Instrum.* **82**, 103501. https://doi.org/10.1063/1.3643771 (2011).
14. Pasch, E. *et al.* The Thomson scattering system at Wendelstein 7-X. *Rev. Sci. Instrum.* **87**, 11E729. https://doi.org/10.1063/1.4962248 (2016).
15. Yoshikawa, M. *et al.* Electron temperature and density measurements by using the Thomson scattering system in the tandem mirror GAMMA 10. *JINST* **8**, C10016. https://doi.org/10.1088/1748-0221/8/10/C10016 (2013).
16. Huang, Y. *et al.* Multipoint vertical-Thomson scattering diagnostic on HL-2A tokamak. *Rev. Sci. Instrum.* **89**, 10C116. https://doi.org/10.1063/1.5035556 (2018).
17. Kim, J. H., Kim, Y. G., Kim, D., Lee, J. H. & Hwang, Y. S. Radial profile measurement with an improved 1 kHz Thomson scattering system on Versatile Experiment Spherical Torus. *Rev. Sci. Instrum.* **92**, 043549. https://doi.org/10.1063/5.0043792 (2021).
18. Iiyoshi, A. *et al.* Overview of the Large Helical Device project. *Nucl. Fusion* **39**, 1245–1256. https://doi.org/10.1088/0029-5515/39/9Y/313 (1998).
19. Takeiri, Y. The Large Helical Device: Entering deuterium experiment phase toward steady-state helical fusion reactor based on achievements in hydrogen experiment phase. *IEEE Trans. Plasma Sci.* **46**, 2348–2353. https://doi.org/10.1109/TPS.2017.2784380 (2018).

20. Yasuhara, R., Sakamoto, R., Yamada, I., Motojima, G. & Hayashi, H. Short-interval multi-laser Thomson scattering measurements of hydrogen pellet ablation in LHD. *Rev. Sci. Instrum.* **85**, 11D822. https://doi.org/10.1063/1.4890251 (2014).
21. Damm, H. *et al.* First results from an event synchronized - high repetition Thomson scattering system at Wendelstein 7-X. *JINST* **14**, C09037. https://doi.org/10.1088/1748-0221/14/09/C09037 (2019).
22. Yoshikawa, M. *et al.* First electron temperature and density measurements using the multi-pass Thomson scattering system with the lase amplification system in GAMMA 10/PDX. *JINST* **15**, T08011. https://doi.org/10.1088/1748-0221/15/08/T08011 (2020).
23. Yoshikawa, M. *et al.* Improvement in multipass Thomson scattering system comprising laser amplification system developed in GAMMA 10/PDX. *Rev. Sci. Instrum.* **92**, 033515. https://doi.org/10.1063/5.0040461 (2021).
24. Meiden, H. J. v. d. *et al.* 10 kHz repetitive high-resolution TV Thomson scattering on TEXTOR: Design and performance (invited). *Rev. Sci. Instrum.* **77**, 10E512. https://doi.org/10.1063/1.2219434 (2006).
25. Den Hartog, D. J. *et al.* Pulse-burst laser systems for fast Thomson scattering (invited). *Rev. Sci. Instrum.* **81**, 10D513. https://doi.org/10.1063/1.3475723 (2010).
26. Den Hartog, D. J. *et al.* Pulse-burst operation of standard Nd:YAG lasers. *J. Phys.: Conf. Ser.* **227**, 012023. https://doi.org/10.1088/1742-6596/227/1/012023 (2010).
27. Den Hartog, D. J., Borchardt, M. T., Holly, D. J., Diallo, A. & LeBlanc, B. A pulse-burst laser system for Thomson scattering on NSTX-U. *JINST* **12**, C10002. https://doi.org/10.1088/1748-0221/12/10/C10002 (2017).
28. He, Z. *et al.* Pulse-burst laser-based 10kHz Thomson scattering measurements. *Plasma Sci. Technol.* **21**, 105603. https://doi.org/10.1088/2058-6272/ab2e30 (2019).
29. Ritt, S., Dinapoli & R., Hartmann, U. Application of the DRS chip for fast waveform digitizing. *Nucl. Instrum. Methods.* **A 623**, 486–488. https://doi.org/10.1016/j.nima.2010.03.045 (2010).
30. Yamada, H. *et al.* Development of pellet injector system for large helical device. *Fusion Eng. Des.* **49–50**, 915–920. https://doi.org/10.1016/S0920-3796(00)00342-2 (2000).
31. Sakamoto, R. & Yamada, H. Observation of Cross-field transport of pellet plasmoid in LHD. *Plasma Fusion Res.* **6**, 1402085. https://doi.org/10.1585/pfr.6.1402085 (2011).
32. Sakamoto, R. *et al.* Cross-field dynamics of the homogenization of the pellet deposited material in Tore Supra. *Nucl. Fusion* **53**, 063007. https://doi.org/10.1088/0029-5515/53/6/063007 (2013).
33. Yamada, I., Narihara, K., Hayashi, H. & LHD Experimental Group. Raman calibration of the LHD YAG Thomson scattering for electron-density measurements. *Rev. Sci. Instrum.* **74**, 1675–1678. https://doi.org/10.1063/1.1538362 (2003).

Acknowledgements

Author contributions

R.Y. proposed, designed, and organized the high-repetition-rate Thomson scattering system in LHD. H.F. analyzed the data. R.Y. and D.J.DH. developed the high-repetition-rate laser and R.Y. and H.U. conducted and operated the laser optical system. I.Y is a responsible person of the LHD Thomson scattering system except the high-repetition-rate laser. I.Y and H.F discussed about the evaluation of T_e and n_e. R.S. operated the pellet injector. M.O. conducted the experiments. H.F wrote the manuscript and all authors reviewed the manuscript.

Competing interests

The authors declare no competing interests.

Additional information

Correspondence and requests for materials should be addressed to H.F. or R.Y.

Reprints and permissions information is available at www.nature.com/reprints.

Publisher's note Springer Nature remains neutral with regard to jurisdictional claims in published maps and institutional affiliations.